Light attenuation as a control for microbiogeomorphic features: Implications for coastal cave speleogenesis

Postprint of: Geomorphology 354: 107054 (2020)

Light attenuation as a control for microbiogeomorphic features: implications for coastal cave speleogenesis

Ilenia M. D'Angeli[1*], Larissa A. Naylor[2], Martin Lee[2], Ana Z. Miller[3,4], John Mylroie[5], Jo De Waele[1]

[1]Department of Biological, Geological and Environmental Sciences, University of Bologna, IT.

[2]School of Geographical and Earth Sciences, University of Glasgow, UK.

[3]HERCULES Laboratory, University of Évora, PT.

[4]Instituto de Recursos Naturales y Agrobiología de Sevilla (IRNAS-CSIC), Seville, ES.

[5] Department of Geosciences, Mississippi State University, USA

*Corresponding author: dangeli.ilenia89@gmail.com

Abstract

San Salvador (Bahamas) is a carbonate island with dozens of flank margin caves formed in the phreatic zone by fresh seawater mixing within the freshwater lens. These caves have no direct connection with the sea, and form at or close to the tidally influenced fluctuating water table. After sea-level fall, in their subaerial parts caves are enlarged mainly by rock dissolution and by erosion close to the water level, condensation-corrosion and breakdown processes. For understanding the geomorphological features observed in these caves and how they are related to light attenuation, we investigated three sampling sites in the tidally influenced zone of Lighthouse Cave, which has been re-invaded by seawater during the Holocene sea-level highstand. A freshwater lens no longer exists within or adjacent to the cave. Rock samples were collected above and below the internal lake shores close to the entrance, and in the twilight and dark zones of this cave. Light and electron microscopy examinations were conducted for detecting microbial cells, as well as bioconstruction and bioweathering features. In addition, a high precision laser scanner was used for characterising

sample microtopography. Our data showed that the microtopography and geomorphology of the lake shore samples (cave entrance) are dominated by bioweathering, whereas the samples of the twilight and dark zones are controlled by a combination of both bioweathering and bioconstructive processes depending on light availability. Bioconstructive structures, such as semi-planar lamination, at the fluctuating water level of the Lighthouse Cave show that dissolution due to water mixing of sea and freshwater in the Holocene is no longer the most important speleogenetic process. We propose that the geomorphological evolution is strongly influenced by the degree of rock diagenesis more than the initial mechanism of speleogenesis.

Keywords: Flank margin caves; mixing dissolution; tides; bioconstruction-bioweathering processes

1. Introduction

San Salvador Island is located in the eastern part of the Bahamas within the Bahamian Archipelago in the Atlantic Ocean (Fig.1A). This island is about 11 km wide and 19 km long and lies in a tectonically stable area, which has been influenced by eustatic sea-level change during the Quaternary. The island is characterised by a sequence of Pleistocene shallow-water carbonate deposits covering the oceanic crust basement (Meyerhoff and Hatten, 1974; Supko, 1977; Carew and Mylroie, 1985). The dissolution of Bahamian carbonates produced karstic features such as karren, shallow depressions, blue holes, and the well-known *flank margin caves* (Roth et al., 2006; Labourdette et al., 2007). *Flank margin caves* (FMC) (Mylroie and Carew,1990; Harris et al., 1995; Gulley et al., 2016) generally present subhorizontal branches that develop at the edge of the freshwater lens where the area of vadose/phreatic water mixing and fresh-seawater mixing zones are superimposed. The water mixing produces a renewed aggressive solution that further dissolves carbonate, thus forming caves (James and Choquette, 1984; Mylroie and Carew, 1995). FMC developed in eogenetic limestone (diagenetically immature carbonate rocks with high primary porosity), such as the case of Lighthouse Cave, have been described from many carbonate islands

(e.g., Mylroie et al., 2001; Vacher and Mylroie, 2002; Mylroie and Mylroie, 2007; Kourampas et al., 2015) and also on carbonate coasts on large islands or continental margins (D'Angeli et al., 2015b; White and Webb, 2015; Bontognali et al., 2016; De Waele et al., 2017, 2018). Nevertheless, FMC can also develop in more highly lithified carbonate rocks (telogenetic limestones) (Mylroie et al., 2008; Otoničar et al., 2010; Ruggieri and De Waele, 2014; D'Angeli et al., 2015a), during past high sea levels.

FMC in eogenetic rocks are mainly characterised by spongy morphologies, maze areas, dead-end passages, cuspate walls and irregular chambers that narrow inland. Presence of phreatic dissolution pockets are common, and the absence of high-velocity structures, turbulent-flow wall sculptures (i.e., scallops) and stream sediments (Waterstrat et al., 2010) indicates a diffuse or laminar flow speleogenetic environment. Wave processes are not required in FMC speleogenesis; exclusively sea level change (mainly due to coastal uplift or eustatic fluctuation) can influence their position (Mylroie and Carew, 1988). These caves form without entrances; access to them and/or the invasion of daylight into them, only occurs post-speleogenesis, when denudational processes breach their tops and/or sides.

It is well known that caves are low energy environments that can preserve fragile speleothems, sediments, and archaeological remains over long time spans (e.g., Van Hengstum et al., 2011; Winkler et al., 2016). In addition, they can host unique microbial communities adapted to subsurface environmental conditions, such as absence of light and low organic matter input (Tomczyk-Żak and Zielenkiewicz, 2016). In general, the cave entrance (strongly influenced by surface conditions) and the twilight zone (with limited light penetration but still important temperature and relative humidity variations) are dominated by phototrophs, whereas the dark zone (characterised by absence of light and stable environmental conditions the year round) is dominated by chemotrophs (Northup and Lavoie 2001; Mejía-Ortíz et al., 2018; Popović et al., 2019). Microorganisms interact with minerals and promote bioweathering (Naylor and Viles, 2002) and biomineralisation processes (Barton and Northup, 2007; Riquelme et al., 2015). They can also have

79 an important, albeit poorly understood, role in ecosystem engineering (Phillips, 2016). The key
80 biogenic and biochemical processes that create distinctive morphological features in caves are: i)
81 microbially-mediated mineral dissolution, and ii) microbially-mediated mineral precipitation
82 (Riquelme et al., 2015). Sulphur, iron and/or manganese oxidising bacteria in contact with
83 carbonate rocks, increasing local acidity through redox reactions and secretion of organic acids or
84 exoenzymes (Sand, 1997), produce intense mineral dissolution (Northup and Lavoie, 2001; Miller
85 et al., 2014) and secondary mineral deposition such as manganese oxides and moonmilk deposits
86 (Hill and Forti, 1997; Gradziński et al., 1997; Miller et al., 2012, 2018). Microbially-mediated
87 precipitation of minerals, especially carbonates, has been frequently observed (Tisato et al., 2015;
88 Bontognali et al., 2016), but more detailed research is needed to better understand the main
89 processes involved. For instance, microalgae and cyanobacteria, growing close to cave entrances or
90 in the twilight zone, can precipitate $CaCO_3$ by fixing carbon dioxide or can trap and bind particles
91 transported by flowing water or wind (Contos et al., 2001). Most interestingly, "crayback" or
92 "lobster" biomediated mineral growth known as "cyanobacterial subaerial stromatolites" (in the
93 twilight zone) have been found in caves in New South Wales, Australia (Cox et al., 1989a, 1989b),
94 and in Borneo (Lundberg and McFarlane, 2011, 2012). Crusts and coatings of iron-oxyhydroxides
95 (Peck, 1986; Provencio and Polyak, 2001; Frierdich and Catalano, 2012) and manganese-oxide
96 crusts have been found on cave walls (Onac et al., 1997; Northup et al., 2000; Lozano and Rossi,
97 2012). These authors demonstrated that rock weathering is influenced by microbial processes
98 (Dotson et al., 1999; Northup et al., 2003). In addition, Onac et al. (2001) and Audra et al. (2019)
99 reported bat guano to be an important source for mineral growth.
100 To date there have been few investigations on the microbially-mediated processes that operate in
101 each cave zone, and how they may affect the type and spatial patterns of morphological features in
102 cave systems (an exception is Coombes et al., 2015). Here we have sought to address some of these
103 knowledge gaps by investigating the microbiogeomorphic processes developing at the entrance,
104 twilight and dark zones of a flank margin cave system (Lighthouse Cave) located in the Bahamas.

105 In addition, we attempted to identify consistent biogeomorphic features and/or processes that can be
106 associated with ecosystem engineering and likely to construction niches sensu Phillips (2016).
107 Hence, the aim of this study was to understand how biological processes can influence eogenetic
108 carbonate rocks in the development of peculiar micromorphological features (e.g., mineral
109 precipitation, pitting/etching, boreholes) in zones of the cave system with different natural light
110 conditions, and assess how present (post-mixing) flank margin cave evolution may be influenced by
111 secondary bioweathering or bioconstruction processes.
112
113 **2. Materials and Methods**
114 **2.1. Site description and sampling**
115 San Salvador Island has a tropical climate, with daily average temperatures of 25-28°C (Gulley et
116 al., 2015), generating a very high potential evaporation rate of > 1300 mm/yr (Crump and Gamble,
117 2004). The Lighthouse Cave is a limestone cave system located on the NE coast of San Salvador
118 Island (The Bahamas) (Fig.1B), and has no direct connection to the sea.
119 The cave is 402 m-long, and half of the passages show water bodies still influenced by tidal
120 fluctuation (1 m range). The water bodies inside the cave have an overall salinity of 33 PSU,
121 conductivity of 52 mS/cm, 26.6°C, and 7.21 pH (McGee et al., 2010). From the geomorphological
122 point of view, the cave is composed of one large central chamber, adjacent smaller halls, and
123 ramifying dead-end branches developed between 2 to 11 m a.s.l., following the flank of a dune, and
124 mainly formed during 5e high stand. The main entrance and two minor entrances are vadose pits
125 created after the flank margin cave speleogenesis. The main morphologies are characterised by a 3D
126 maze and a tubular branch ending abruptly, domes, arches; big halls alternate with small and narrow
127 passages, and bell holes are clearly visible on the ceilings. Bat guano deposits are abundant in the
128 twilight zone, close to the cave entrance, and represent the most important source of organic matter
129 and phosphate minerals in Lighthouse Cave (Onac et al., 2001).

130 Cave walls are generally white, but dark brown crusts are also visible along the tidal zone (Mylroie,
131 2014). Three replicates from the three different sampling sites (Fig. 2) were collected in Lighthouse
132 Cave in February 2014 during low tide (local tidal vertical range of ~0.80 m). Three cm-long rock
133 samples were taken using a geologist hammer and stored in sterile plastic bags. All the rock
134 samples were collected from calcarenitic eolianite limestone belonging to Owl's Hole Formation
135 (Middle Pleistocene age) (Panuska et al., 1999; Kindler et al., 2010). The sampling sites were: i) a
136 limestone rock exposed in the intertidal zone of a hypersaline lake located in a mangrove forest, 20
137 m W of the main cave entrance (sampling site: SS1); ii) a limestone wall in the twilight zone of the
138 cave, 20 m from the entrance, close to the water table, approximately 10-15 cm below mean high
139 tide level (sampling site: SS2), and iii) a limestone wall near the water table, approximately 25 cm
140 below high tide level and located ~60 m from the cave entrance (sampling site: SS3).
141
142 **2.2. Microtopographic characterisation**
143 To identify the processes involved in the present-day cave evolution, the millimetre-scale
144 microtopographic irregularities of each rock sample were examined using a high-precision laser
145 scanner. This instrument minimises measurement errors and resolution problems associated with
146 conventional roughness meters (Bourke et al., 2008), and creates digital terrain models (DTMs). We
147 used a micro Epsilon high-precision laser scanner at the University of Glasgow, with a maximum
148 distance between the laser and sample of ~35 mm. Contour map analyses were performed using the
149 ArcGIS system. Six profiles (NNE-SSW) were drawn across each rock sample (using a systematic
150 random sampling design) to measure roughness values (Giaccio et al., 2002; Gomez-Pujol et al.,
151 2006; Naylor et al., 2012; Moses et al., 2014). Roughness values were obtained using the following
152 ratio, after Whitehouse (2012):

$$\frac{Surface\ length\ (mm)}{Profile\ length\ (mm)}$$

153
154 **2.3. Stereomicroscopy and ESEM analysis**

155 Stereomicroscopy and Environmental Scanning Electron Microscopy (ESEM) investigations were
156 performed to observe newly formed crystals and recognise microbial communities that contributed
157 to microtopographic changes on the rock surfaces (Moses et al., 2014; Coombes et al., 2015). These
158 observations were conducted at the University of Glasgow, based on the methods of Naylor and
159 Viles (2002) and Coombes et al. (2011, 2015). Three rock chips, ~4 cm^2, were studied at each
160 sampling site (Table 1) to generate semi-quantitative data on biogeomorphological processes
161 operating in each zone of the cave system. The top surface of each chip was observed using
162 Olympus SZ x7 and Olympus Bx41 microscopes equipped with an Olympus DP25 camera for the
163 recognition of biological features, such as photosynthetic-based biofilms, shiny filaments, fossils,
164 white creamy deposits, and black coatings (after Naylor and Viles, 2002, and Coombes et al., 2011,
165 2015). Ten random replicate points (without overlap) were chosen on each chip and studied at three
166 magnifications (×2, ×3.2 and ×5.6), which were the most suitable for capturing the spatial variation
167 in organisms across all three sampling zones.
168 The top surface and a cross-section of each chip were subsequently studied using a FEI Quanta
169 200F Environmental SEM, operated at 20 kV, and equipped with a EDAX Energy Dispersive X-ray
170 spectrometer (EDS). The chips were uncoated as they were observed in low vacuum mode.
171 Secondary electron (SE) and backscattered electron (BSE) images were acquired. Ten replicate
172 points on the top surface of each rock chip were selected randomly (without overlap) to study the
173 occurrence of bioconstructions (e.g., biochemical encrustations, extracellular polymeric substances
174 (EPS), microbial filaments, algae, foraminifera, minerals) and bioweathering features (e.g.,
175 microboring, dissolution features, microcracks, biological pitting/etching). Likewise, six replicate
176 points (without overlap) were chosen from each chip to analyse the same features in cross-section.
177 The occurrence of features observed by stereomicroscopy and ESEM were classified using
178 "SACFOR" abundant scale (Hiscock, 1996) with the following classification: superabundant (80-
179 100%), abundant (40-79%), common (20-39%), frequent (10-19%), occasional (5-9%), rare (1-4%)
180 and absent (0%). This method is used to describe and quantify the abundance of marine benthic

flora and fauna in biological surveys (Jones and Pinn, 2006; Howarth et al., 2011). It has been also employed in the analysis of micro-scale biological growths involved in weathering and erosive processes of engineering materials (Coombes et al., 2011).

2.4. Statistical analysis

Statistical analyses were conducted for the recognition of microbial patterns related to different natural light conditions throughout the cave system and for understanding the intensity of bioweathering and bioconstructive processes. The occurrence of biological features in the three sampling sites (SS1, SS2, SS3), as observed by stereomicroscopy, were first tested for normality and subsequently analysed using the ANOVA method to check for homogeneity of variance (Table 1) (Underwood, 1997; Coombes et al., 2011). Each biological feature observed with stereomicroscopy (i.e., algae, shiny filaments, fossils, white creamy deposits, black coatings) was treated as a fixed factor and analysed for all "sampling sites" (SS1, SS2, SS3) and magnifications (×2, ×3.2, ×5.6) using an Excel data sheet. Sampling sites and magnifications are the two sources of variation. The comparison of combined "Sampling site observations" x "Magnification observations" was made using the analysis of variance: single factor.

Biological features observed by ESEM were also analysed (Table 1). We treated each sampling site individually, separating bioconstructive from bioweathering features and analysed them using the *t*-Student test (two tailed test: two-samples assuming unequal variance) in two situations (on the top surface and in cross-section) to understand if their presence is influenced by a specific location and factor.

3. Results

3.1. Rock microtopography

The microtopographic analysis performed for all rock samples collected in Lighthouse Cave revealed differences in the surface microreliefs according to their location. The contour map

207 analysis showed how microtopography changed within the different cave zones. For each rock
208 sample (one chip per sampling site; see Table 1), five distinctive classes of microrelief were
209 established (Table 2): i) sample SS1, located on a karren stone in the intertidal zone of a hypersaline
210 lake, depicted three classes of relief, ranging from 0 to 4-8 mm; ii) in SS2, collected in the twilight
211 zone of the cave, we observed the whole range of relief classes (from 0 to >12 mm), and iii) sample
212 SS3, from the dark cave interior and with the smallest range of roughness values (mean roughness
213 1.08), four classes of relief (from 0 to 8-12 mm), were noticed (Table 2).
214
215 **3.2. Microscopy observations**
216 Different biological features were observed by stereomicroscopy at three different magnifications
217 (Fig. 3), comprising filaments of staghorn-like algae (Fig. 3A), biofilms of green algae (Fig. 3B)
218 and biological-like filamentous structures (Fig. 3C). The occurrence of biological features tended to
219 decrease from site SS1 towards SS3 (Fig. 4), whereas the shiny filaments (Fig. 3D), fossils (Fig.
220 3E), and black coatings (Fig. 3F) tended to increase towards the cave darkness (Fig. 4). Brown
221 coatings were reported in all samples. The occurrence of these biological structures was measured
222 as shown in Figure 4, based on the SACFOR scale. Magnification of x5.6 revealed the most
223 representative results across all the studied sampling sites. Brown and black coatings showed the
224 highest occurrence for all the studied samples, contrasting with generic red algae and fossils.
225 *Cladophora* algae, white creamy deposits and black coatings were solely observed in SS1, SS2 and
226 SS3, respectively (Fig. 4).
227 White creamy deposits (Fig.5A, 5B) were exclusively observed on the chips collected from site
228 SS2, and are preferentially located along the depressions on the exposed rock surface (Fig.5A). The
229 EDS microanalysis showed that the creamy white deposits contain the following elements: C, O, Cl,
230 P, Mg, Ca, Na, S, Al, Si, K, Fe, and Mn (see the green spot in Figure 8).
231

232 ESEM examinations were performed on three chips per sampling site, and the occurrences (%) of
233 bioconstructive and bioweathering features both on the top surface and in cross-section are reported
234 respectively in Figure 6 and 7. Generally, bioweathering features were more abundant in the chip
235 cross-section, probably due to the biological coating observed on the top surface hiding the
236 dissolution structures.
237 ESEM images of bioconstructive and bioweathering features are reported in Figure 8. EDS
238 microanalyses showed that sample SS1 is composed of microcrystalline calcite (Fig. 8B and
239 corresponding EDS spectra), with abundant salt crystals due to the presence of seawater in the
240 sample location (Fig. 9A). It was noticed that when biological crusts are less abundant on the
241 sample surface, salt can easily penetrate up to a depth of ~3.5 mm (Fig. 9). In contrast, when
242 extensive microbial mats are present on the sample surface, biological pitting and etching solely
243 extend to a depth of 1-1.5 mm (Fig. 9A). Sample SS2 is characterised by an overall porosity of 12%
244 and shows the presence of several layers (Fig. 5C), the yellowish layers seem to be more compact
245 (made of microcrystalline calcite crystals), whereas the white layer is composed of calcite with
246 copious borings, likely contributing to enhance its porosity (Fig. 5D). Fine layers and aggregates of
247 Ca-phosphate minerals are present both along the cross-section and on the sample surface, and are
248 likely related to bat guano deposits. Borings of approximately 0.5 mm diameter are clearly visible
249 along the cross-section, increasing mineral porosity (Fig. 9B).
250 The top surface of SS3 is characterised by cubic Ca-phosphate minerals (Fig. 8K and Fig. 9C) and
251 black coatings of ferromanganese oxides, whereas the inner part is made of carbonate minerals
252 enriched in Mg and acicular Ca-phosphates (Fig. 8J and Fig. 9C). Endolithic microorganisms able
253 to pit and etch rocks were also observed (Fig. 8I).
254 Table 3 summarizes and compares all the results obtained for the rock chips from each sampling
255 site.
256 The results of the ANOVA analysis for the biological features observed by stereomicroscopy are
257 reported in Table 4. The null hypothesis affirms: “The biological features are not influenced by light

attenuation". The obtained results show $F_{values} > F_{critic}$ in almost all biological features of the three sites. This result means that the null hypothesis can be rejected because the distribution of almost all the observed biological features is influenced by light attenuation. Only the brown coatings show an $F_{value} < F_{critic}$, suggesting that their distribution is not influenced by light attenuation.

The results of Student's *t*-test analysis of ESEM observations are reported in Tables 5 and 6 (bioconstructive and bioweathering features, respectively). We used Student's *t*-test to understand whether bioconstructive-dissolution features related to the same process. Analysing bioconstructive features on the top surface and cross-sections from the three sampling sites showed that the P (probability) values for SS1 and SS2 are higher (Table 5) than the critical value (0.05). This result means that the *t*-test analysis is not significant and so it is difficult to reject null hypothesis.

Bioconstructive features in SS1 and SS2 could be related to the same process (i.e., the presence of blue filaments). Conversely, the P value of SS3 is lower (Table 4) than the critical value (0.05), so null hypothesis can be rejected because the bioconstructive features might be related to a different process (i.e., the presence of shiny filaments or Mn-Fe oxide-hydroxide precipitation). Analysing bioweathering features, we saw that P values are much higher (see Table 6) than P critical value (0.05), demonstrating the test analysis not to be significant. The same process (i.e., the presence of microorganisms able to pit and etch the rock) can be responsible for the observed phenomena.

4. Discussion

Contrasts in light attenuation inside the cave have an important influence on biological colonisation. Based on visual inspections and microscopy observations, sampling sites SS1 and SS2 are dominated by phototrophic organisms. Their behaviour affects microtopography, mineralogy and geochemistry of the rock substrate.

We sought to assess how the micromorphology of karst environments changes across an environmental and process gradient. Biological features occur in all samples, and three different associations were recognised using light and scanning electron microscopy, one for each sampling

site. We observed that blue filaments, *Cladophora* and red algae (including staghorn algae) tend to decrease in abundance from the hypersaline lake toward the cave interior owing to light attenuation, whereas shiny filaments, fossils and black coatings tend to increase along the same profile. This result agrees with Coombes et al. (2015), who studied the Puerto Princesa Underground River in the Philippines, suggesting that the sensitivity of microbial communities to light strongly influences the nature and types of biogeomorphological processes that operate in cave systems.

The increase of fossils (in SS3) is related to a marine inflow (through fractures), whereas shiny filaments and black Mn-coatings might be controlled by microorganisms able to thrive in nutrient-poor dark locations.

Light attenuation plays an important role in influencing the behaviour of biological communities involved in landform processes, bioweathering and bioconstruction within the underground environment. As suggested by Phillips (2016), light attenuation is an interesting candidate for "niche construction". Niche construction means that biogeomorphic ecosystem engineering influences natural selection (such as stromatolite formation and/or Ca-nitrate precipitation in dry cave deposits). As a matter of fact, it is well-known that geomorphic processes (such as cementation-precipitation, weathering, erosion and deposition) can be both microbially-controlled, -induced, –influenced, and/or abiotic (Viles, 2012).

To provide a clear understanding, the data obtained in this study are separately discussed for each sampling site, focusing on the main biogeomorphological processes.

4.1. Sampling site SS1

The microtopography and high surface roughness of the limestone rock from sampling site 1, located in a hypersaline lake near the cave entrance, were promoted by biological activity as revealed by microscopy observations (boreholes and pittings). On the top surface of SS1 we also observed a salt penetration band (~6 mm), as well as changes in rock porosity associated with endolithic growth. It is well known that salt crystallisation, similar to microgelivation, can actively

310 contribute to the weathering of rocks, especially through its penetration into pore spaces and rock
311 fractures (Williams and Robinson, 1998; Matsuoka, 2001; Moses et al., 2014). The depth of
312 subsurface deterioration depends on parameters such as porosity, permeability, lithology and
313 moisture, as well as climatic conditions and biological activity (Matsuoka, 2001). Epilithic
314 organisms may weaken the top surface of rocks (e.g., by boring, pitting and etching), whilst the
315 endolithic ones (as observed in SS3 samples) may affect the rock just beneath the surface by
316 enlarging porosity or fractures, through chemical-physical reactions that change their
317 microenvironment (Friedmann, 1982; Bell, 1993; Viles, 2000; 2012). Phototrophs were the
318 dominant organisms colonising the rock surface in SS1, and, likely helped by salt penetration and
319 gastropod grazing activities, contributed in weakening and disaggregating particles, which were
320 subsequently removed by seawater (wave and tide fluctuations) and/or by wind. These processes
321 together would have created the observed profile characterised by microvalleys and -ridges.
322
323 **4.2. Sampling site SS2**
324 The SS2 rock chips showed greater roughness (Table 2), and their profile is more pronounced than
325 SS1 (Table 3). The white creamy deposits observed along the depressions of the chip surface, with a
326 complex chemistry (O, Cl, C, P, Mg, Ca, Na, S, Al, Si, K, Fe, and Mn), are likely related to bat
327 guano deterioration. The fine layers and the presence of aggregates of Ca-phosphate minerals
328 associated with the white deposits support this hypothesis. The rock samples from SS2 are
329 characterised by laminae with different colours and porosity/permeability as previously described.
330 The yellowish layers (first and third) (Fig. 9C) are relatively more compact (made of
331 microcrystalline calcite) and less porous than the second whitish layer in which boreholes occur
332 extensively (diameter of 10 ± 4 μm). These microcrystalline layers may be the product of
333 subsequent weathering processes that also changed the primary porosity (Winkler, 1997; Nicholson,
334 2001; Tuğrul, 2004).

335 Black (1933) described deposits in Andros Island (Bahamas) whereby trapping and binding
336 processes involved the presence of cyanobacteria. Thus, the laminations are likely related to
337 trapping and binding of detrital grains and microfossils supplied by tidal fluctuation and recall
338 microbialites (Burne and Moore, 1987). Similar dark-brown and reddish crusts were observed along
339 the intertidal zone in several flank margin caves in Croatia (e.g., Otoničar et al., 2010) and are likely
340 related to microorganisms such as bacteria and red algae. These laminated deposits can be defined
341 as a "biological boundstone" according to Black (1933). The organisms involved in its formation
342 live in dark, quiet, shallow water, and in the tide-influenced twilight zone of the cave environment,
343 where nutrients are delivered by guano that also behaves as source of acids and organic matter
344 input. The extensive borings in the whitish layer of the SS2 chip cross-section suggests that
345 endolithic microorganisms were involved in the formation of these layers (Fig.5D).
346
347 **4.3. Sampling site SS3**
348 The sampling site SS3 is located in the deepest and darkest part of Lighthouse Cave. The top
349 surfaces of SS3 chips showed smoother texture than samples SS1 and SS2 as revealed by high
350 precision laser scanner measurements (Table 4). Black coatings were observed on the sample
351 surfaces, mainly composed of cubic Ca-phosphate minerals and Mn-Fe oxides-hydroxides. In
352 addition, shiny filaments and microfossils were visible. The internal structure of SS3 chips was
353 characterised by porous carbonate minerals enriched in Mg, and acicular Ca-phosphates with pitted
354 and etched crystal surfaces, likely caused by endolithic microorganisms. Similar deposits have been
355 described by Spilde et al. (2009) and were defined as "Speleosols" (i.e., "soil-like materials formed
356 in caves"). They are made of ferromanganese deposits related to two different processes involving
357 the activity of Mn-Fe oxidising and acid-producing microbiological communities (Spilde et al.,
358 2005; Miller et al., 2012): 1) alteration of the cave wall, leaching of soluble elements and
359 subsequent enrichment in Al, Fe, Mn and trace elements, and 2) deposition of secondary minerals
360 (mainly Mn-Fe oxides-hydroxides). Usually these structures have three components: an external

dark-coating/crust or speleosol, a punk rock (a porous and altered portion of host rock; Hill, 1987) and bedrock.

5. Conclusions

Microtopography of the exposed rock surfaces within and close to Lighthouse Cave varies with location (e.g., entrance, twilight zone or deep into the cave). Going from outside (SS1) to deep inside (SS3) there is a general flattening of microrelief.

In general, light attenuation, together with organic matter supply, rock type, age, and diagenetic maturity play an important role in influencing the behaviour of biological communities involved in rock surface processes. We found that bioweathering is more intense on samples collected outside the cave (SS1), likely due to the presence of phototrophs that, dissolving and weakening the rock, disaggregate particles that are subsequently removed by wind erosion, creating typical ridges and valleys in the rock surface microtopography. Nevertheless, episodic gastropod grazing actions might "reset and shape" the overall microtopography. Conversely, within the cave environments, chemotrophs facilitate both bioweathering (endolithic boreholes) and bioconstructive processes by dissolving mineral grains and/or inducing secondary mineral precipitation (e.g., Mn-Fe oxides-hydroxides), respectively.

The above described biogeomorphological structures, especially the ones found along the cave walls (SS2-SS3) at the fluctuating water level, testify that, nowadays in this peculiar flank margin cave, dissolution/corrosion processes due to fresh seawater mixing are less active.

In addition, we propose that the geomorphological evolution is strongly influenced by the degree of rock diagenesis (eogenetic (immature) limestones in Lighthouse Cave vs. telogenetic (mature) limestones of Puerto Princesa Underground River) more than the initial mechanism of speleogenesis.

Acknowledgements

Samples were taken by J. De Waele under co-author John Mylroie's research permit granted by the Bahamas Environment, Science and Technology Commission (BEST Commission) through the Gerace Research Centre, permit numbers G-102 and G-180. Thanks to Arthur and Peggy Palmer for the photographic record made in the Bahamas flank margin caves. This work has benefited from a travel grant from GeoRepNet (I.M. D'Angeli), based at the University of Edinburgh. The support given by Adrienne McCartney in Glasgow has been much appreciated. Thanks to Peter Chung and Paula Lindgren for their help with SEM facilities. We thank Les Hill for the detailed pictures of the chips. I.M. D'Angeli acknowledges Giulia Barbieri for the identification of microfossils (foraminifera). A.Z. Miller acknowledges the support from the CEECIND/01147/2017 contract funded by Fundação para a Ciência e a Tecnologia (Portugal). Funding was also provided by the Spanish project MINECO CGL2016-75590-P with ERDF funds.

399

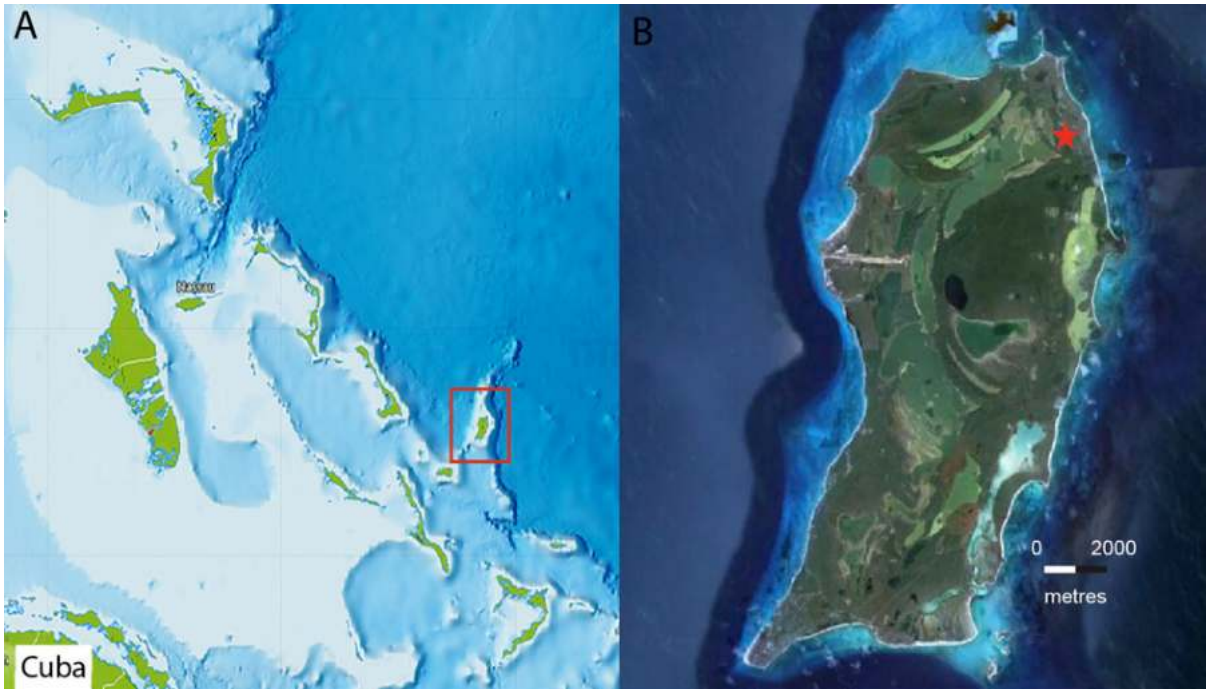

400

401 Figure 1.

402

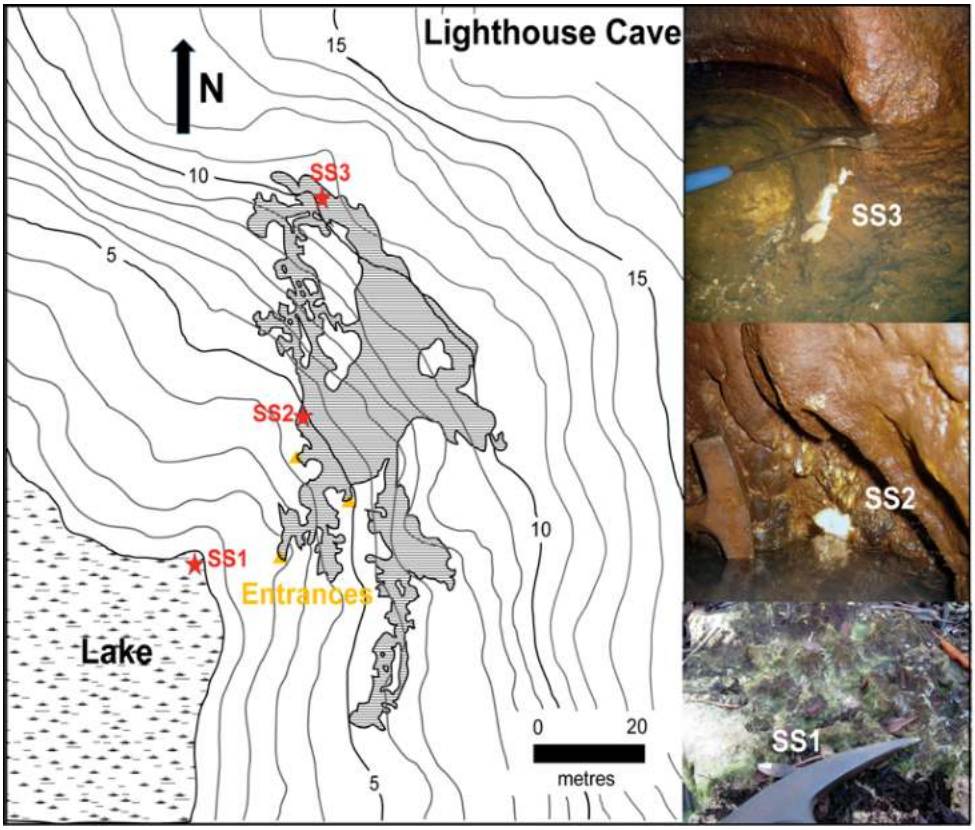

403

404 Figure 2.

405

406 Table 1.

Method	Number of chips studied from each sampling site	Number of observations per chip
Laser scanner	1	1
Roughness measurements	1	6
Light microscopy	3	10
ESEM (surface)	3	10
ESEM (cross-section)	3	6

407

408 Table 2.

Sampling site	Stereomicroscopy image	DTM Contour map analysis	Microrelief classes scale	GIS Contour Map Analysis		Surface roughness value and representative profile
				Total area [mm^2]	**Total area (%) per microrelief class**	
SS1				407 ±3	1) 36.0 ±0.5 2) 53.0 ±0.3 3) 11.0 ±0.2 4) 0 5) 0	1.15 – 1.33 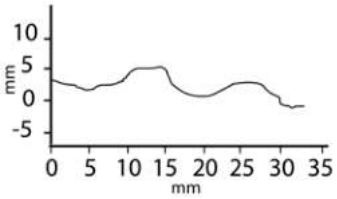
SS2				369 ±6	1) 13 ±0.8 2) 1.5 ±0.8 3) 15.0 ±2 4) 51.5 ±0.6 5) 19.0 ±0.07	1.43 – 2.17 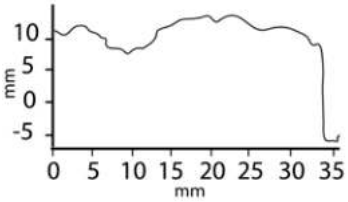
SS3		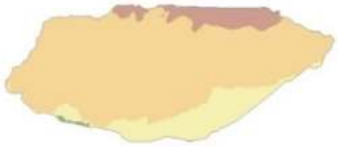		382 ±2	1) 0.4 ±1 2) 15.0 ±0.2 3) 77.0 ±0.3 4) 7.6 ±0.09 5) 0	1.03 – 1.13 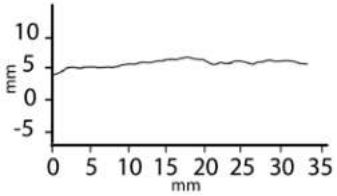

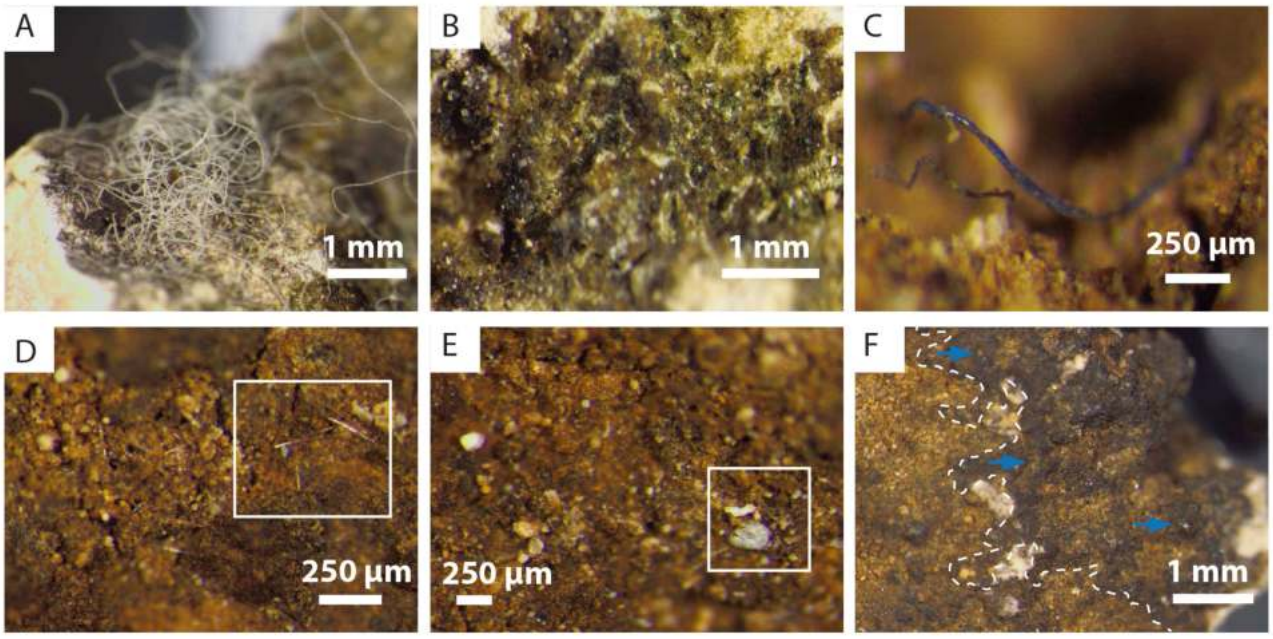

409
410 Figure 3.

411

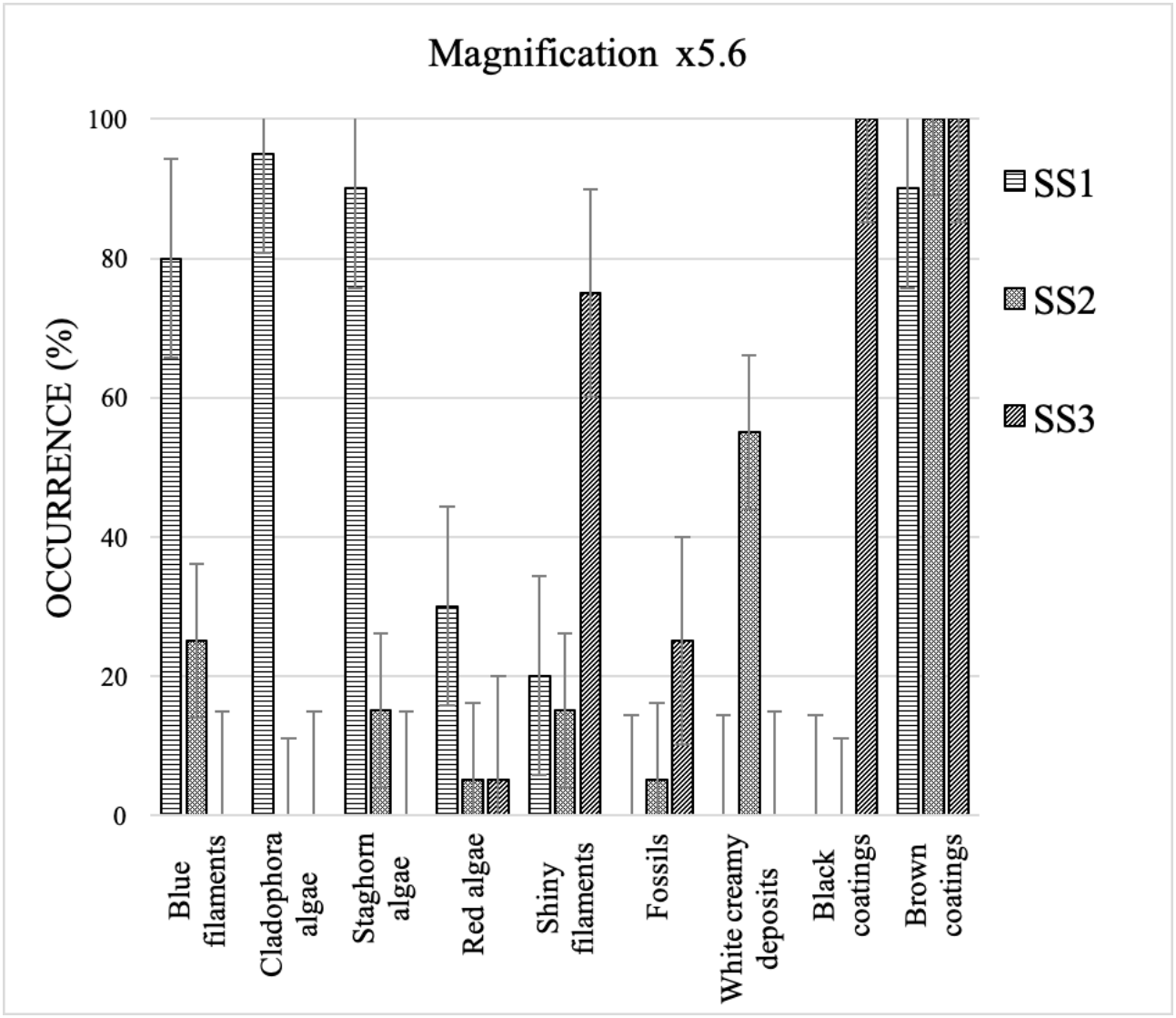

412

413 Figure 4.

414

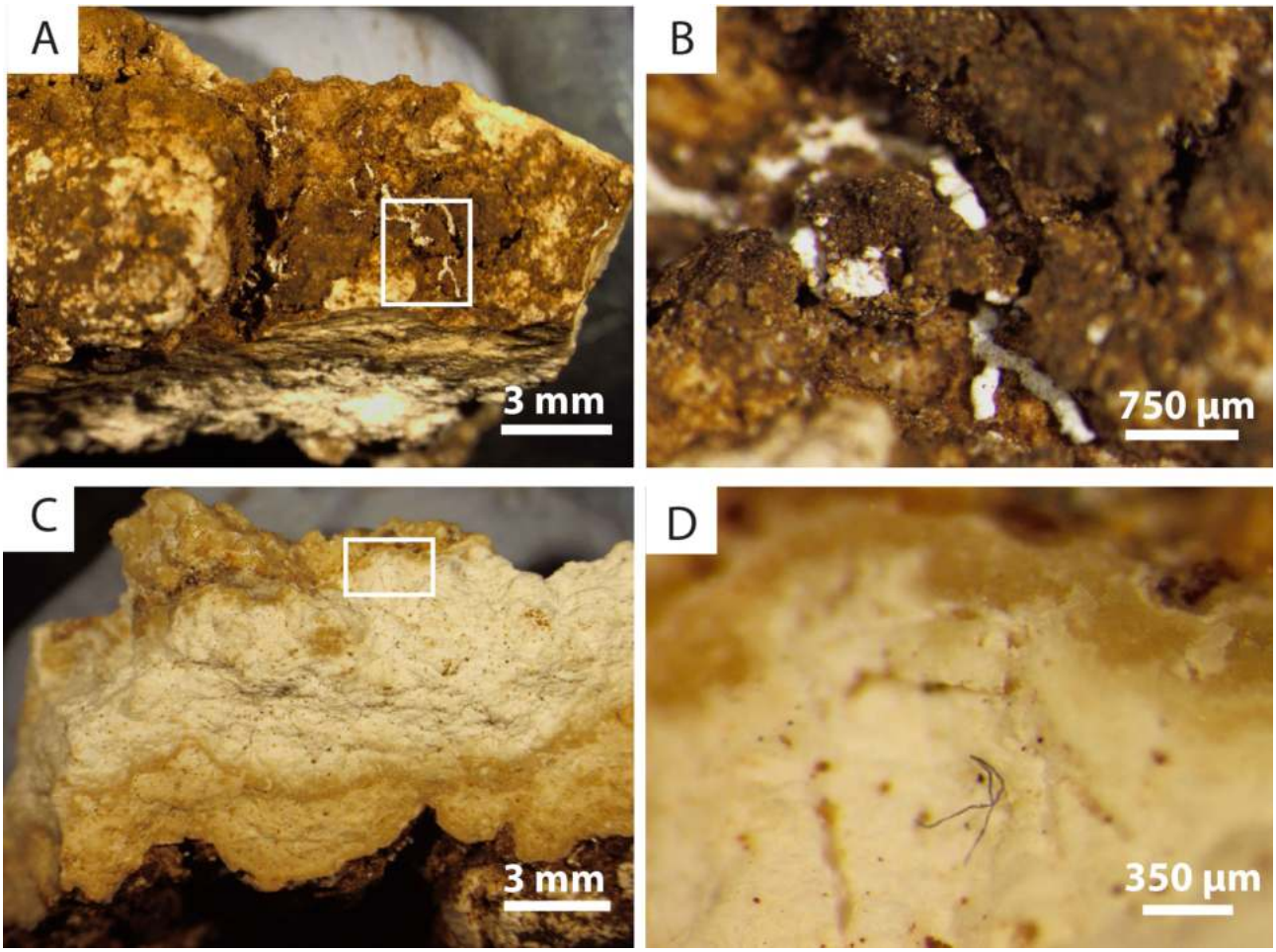

Figure 5.

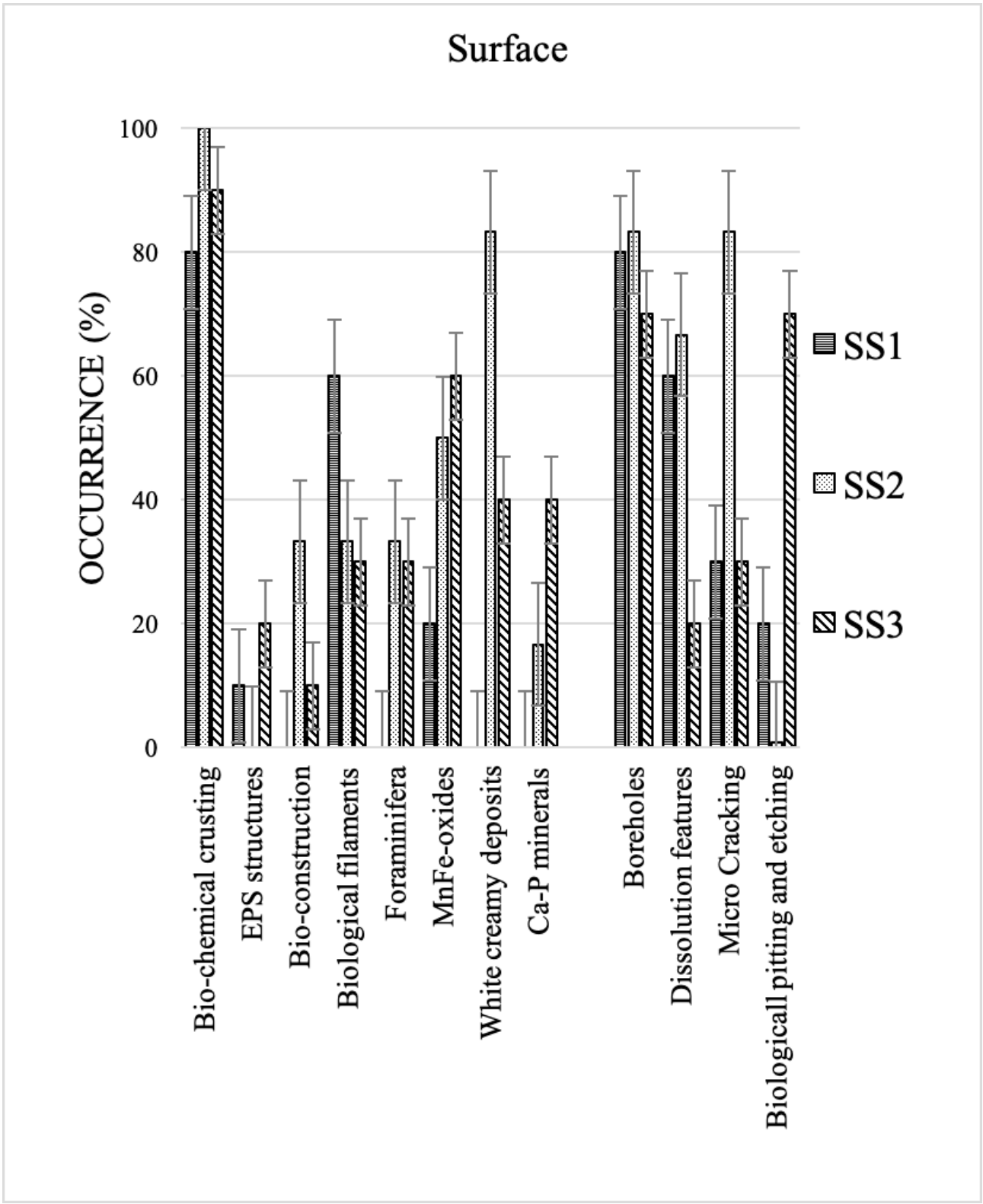
Surface
OCCURRENCE (%)
100
80
60
40
20
0
SS1
SS2
SS3
Bio-chemical crusting
EPS structures
Bio-construction
Biological filaments
Foraminifera
MnFe-oxides
White creamy deposits
Ca-P minerals
Boreholes
Dissolution features
Micro Cracking
Biologicall pitting and etching

Figure 6.

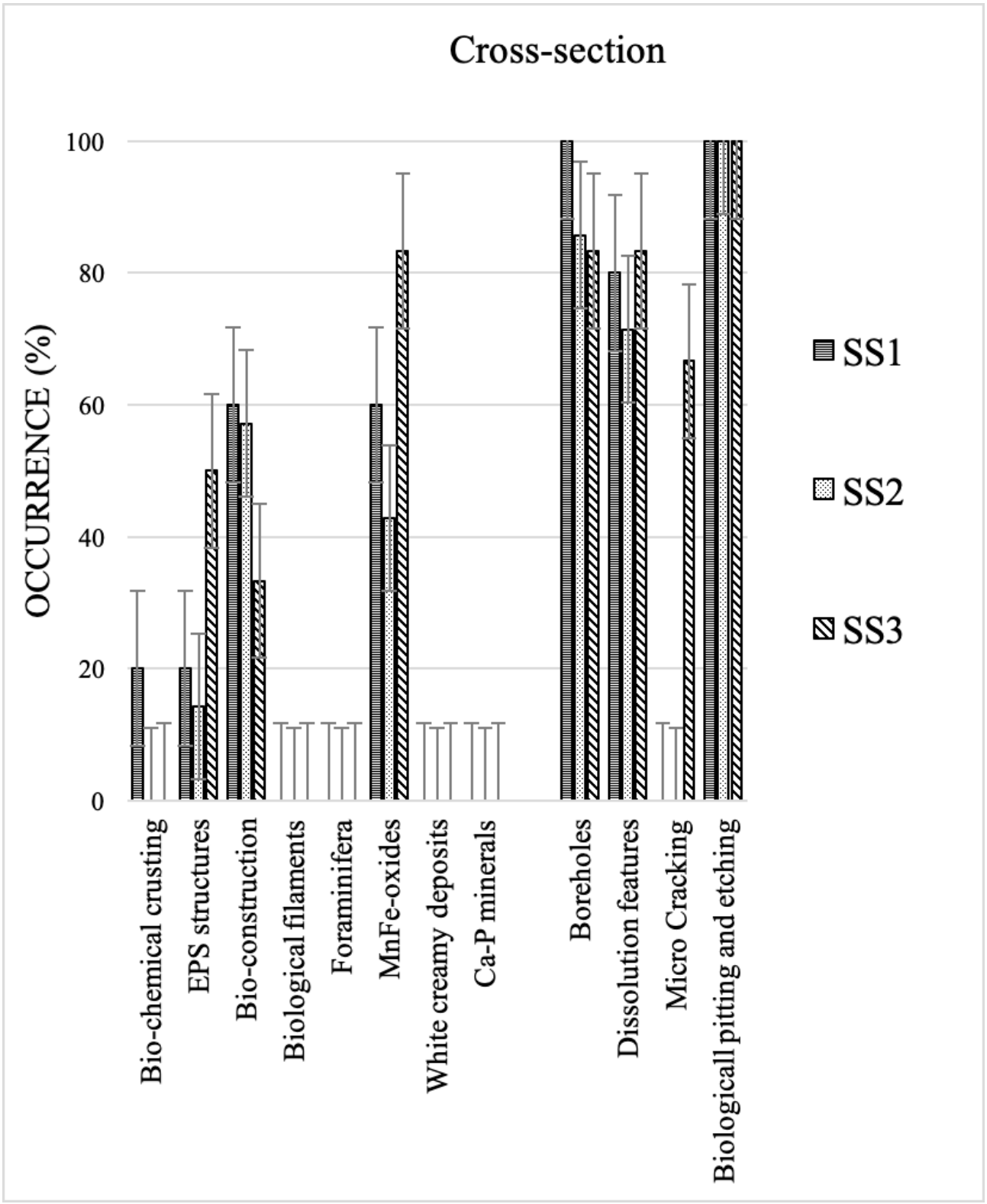

421

422 Figure 7.

423

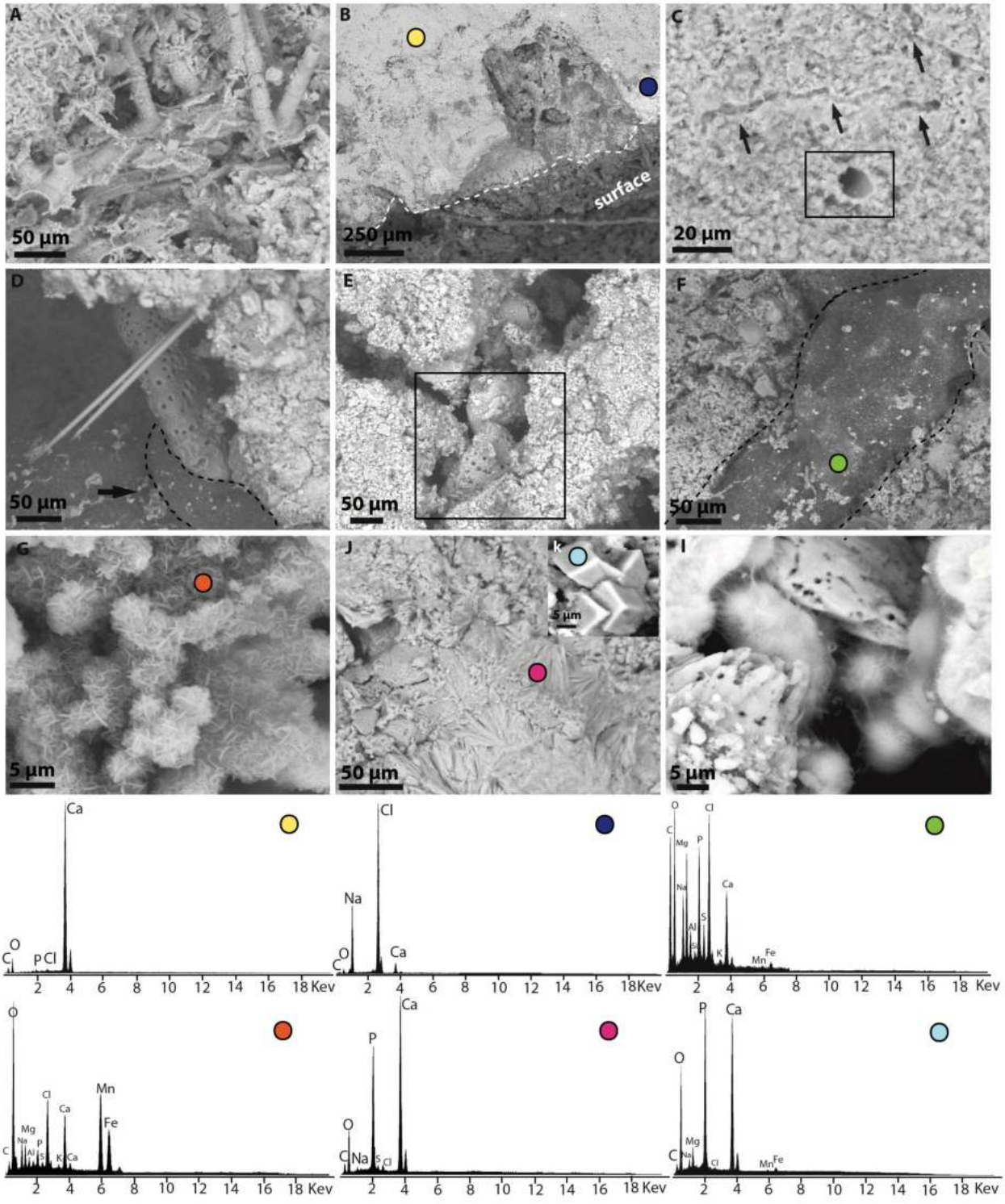
A
50 µm
B
250 µm
surface
C
20 µm
D
50 µm
E
50 µm
F
50 µm
G
5 µm
J
50 µm
k
5 µm
I
5 µm
Ca
O
C
P Cl
2 4 6 8 10 12 14 16 18 Kev
Cl
Na
O
C
Ca
2 4 6 8 10 12 14 16 18Kev
O
C
Mg
Na
P
Al
S
Cl
Ca
K
Mn
Fe
2 4 6 8 10 12 14 16 18 Kev
O
C
Mg
Na
P
Al
S
Cl
Ca
K
Mn
Fe
2 4 6 8 10 12 14 16 18 Kev
Ca
P
O
C
Na
S Cl
2 4 6 8 10 12 14 16 18 Kev
P
Ca
O
C
Mg
Na
Cl
Mn
Fe
2 4 6 8 10 12 14 16 18 Kev

Figure 8.

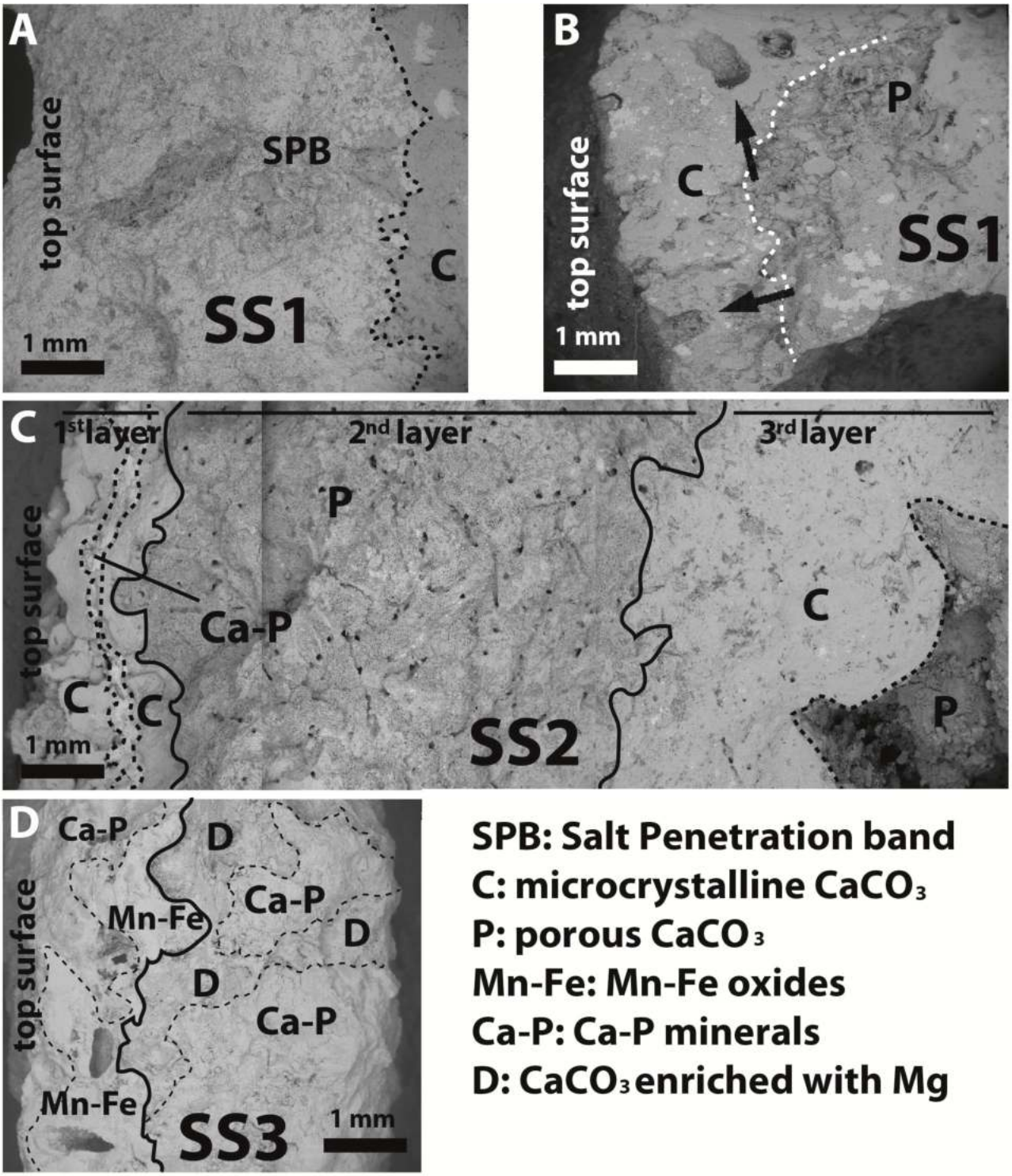

427

428 Figure 9.

429

430 Table 3.

	SS1	SS2	SS3
Sampling Site	• hypersaline lake located in a mangrove forest 20 m W of the main cave entrance	• limestone wall in the twilight zone of the cave, 20 m from the entrance, close to the water table, approximately 10-15 cm below mean high tide level	• limestone wall near the water table, approximately 25 cm below high tide level and located ~60 m from the cave entrance
Rock Characteristics	• Salt penetration band • Pitted and etched band	• Semi-parallel laminae (yellowish and whitish) • Endolithic microboring	• Black coatings of Mn-Fe oxides-hydroxides covering Mg-enriched carbonate rocks
Rock Properties	• Salt minerals promote rock weathering and changes in porosity and permeability	• Creamy deposits (O, Cl, C, P, Mg, Ca, Na, S, Al, K, Fe, Mn) • Ca-phosphate minerals	• Ca-phosphate minerals • Mn-Fe oxides-hydroxides • Fossils
Weathered Rind	• Green brownish crust	• Brown-reddish crust and depression filled by creamy white deposits	• Dark-brownish crust and black coatings
Dominant Microbial features	• *Cladophora* algae • Staghorn algae • Red algae • Blue filaments • Brown coatings	• Red algae • Brown coatings	• Brown coatings • Likely microbial organisms associated with shiny filaments
Microtopography (Roughness value = RV)	• Valleys and Ridges • RV 1.15-1.33	• Well-developed ridges and troughs • RV 1.43-2.17	• Flat surface • RV 1.03-1.13

431

432

433 Table 4.

Biological features	df W	df B	ms W	ms B	F crit	F	*P*
Blue filaments	6	2	8	416	5.14	156	<0.000
Cladophora algae	6	2	5	624	5.14	401.28	<0.000
Staghorn algae	6	2	3	644	5.14	724.75	< 0.000
Red algae	6	2	19	150	5.14	23.31	0.0015
Shiny filaments	6	2	33	202	5.14	18.24	0.0028
Fossils	6	2	8	16	5.14	5.61	0.042
White creamy deposits	6	2	<1	213	5.14	961	<0.000
Brown coatings	6	2	2	2	5.14	3	0.125

434

435

436 Table 5.

Bioconstructive fts.	df	Ms	Mc	Vt	*t*-crit	*t*-value	P
SS1	16	2.2	0.9	5.2	2.12	1.25	0.23
SS2	16	2.4	0.9	3.1	2.12	1.88	0.08
SS3	16	3.5	1.1	5.3	2.12	2.25	0.04

437 df = Degrees of freedom; Ms = mean bioconstructive features observed on the top surface; Mc = mean bioconstructive
438 features observed along the cross-section; Vt = total variance; t-crit = *t* value critic; *t*- value = *t*- value obtained from
439 statistical analysis; P = probability.

440

441

442 Table 6.

Bioweathering features	df	Ms	Mc	Vt	*t*-crit	*t*-value	P
SS1	6	4.7	3.5	6.6	2.44	0.68	0.52
SS2	6	4.7	4.5	4.9	2.44	0.16	0.87
SS3	6	4.7	5	3.8	2.44	-0.18	0.86

443

444

445 **Figure and table captions**

446 Figure 1. A) Location of San Salvador Island, Bahamas, and B) Lighthouse Cave on the NE coast of
447 San Salvador (the red star shows the position of the cave).

448

449 Figure 2. Lighthouse Cave plan (modified from Roth, 2004) and location of sampling sites above
450 present sea level (red stars). The images on the right show the sampling sites SS1, SS2, SS3.
451 Hammer represents the scale of the pictures.

452

453 Table 1. Number of rock chips and observations performed for each analysis.

454

455 Table 2. Contour map analysis of rock samples from each sampling site. The most representative
456 rock chip is shown using stereomicroscopy and DTM images. In addition, microrelief classes scale
457 (1. green, 2. yellow, 3. orange, 4. brown, 5. white), the respective area for each microrelief class, the
458 surface roughness, and representative profile are also reported.

459

460 Figure 3. Biological features observed by stereomicroscopy. A) Site SS1: staghorn algae (red algae)
461 and *Cladophora* algae are clearly visible; B) Site SS1: *Cladophora* algae; C) Site SS2: blueish
462 biological-like filament; D) Site SS3: several tiny shiny filaments are clearly visible in the white
463 square; E) Site SS3: a small fossil (juvenile stage foraminifera) is visible against the brownish
464 background; F) Site SS3: black coatings (blue arrows).

465

466 Figure 4. Occurrence of micro-scale biological features observed by stereomicroscopy (x5.6). Three
467 chips were analysed per sampling site (SS1, SS2 and SS3). Ten points were observed on each chip
468 (without overlap), giving thirty points for each sampling site (at x5.6 the area of an analysed spot is
469 6 mm^2). An occurrence of 100% means that a biological feature is observed in all ten points of each

chip. These measurements were based on the SACFOR scale: superabundant (80-100%), abundant (40-79%), common (20-39%), frequent (10-19%), occasional (5-9%), rare (1-4%) and absent (0%).

Figure 5. Stereomicroscopy images of site SS2; A) White creamy deposits located along the depressions on exposed rock surfaces. B) Detail of A; C) Cross-section of SS2 showing several layers with different colours; the whitish layer is extensively bored; D) Detail of C showing microboring.

Figure 6. Histogram showing the occurrence of bioconstructive and bioweathering features observed on the chip top surfaces from each sampling site (SS1, SS2 and SS3). We analysed three chips from each sampling site, using ESEM.

Figure 7. Histogram showing the occurrence of bioconstructive and bioweathering features along the chip cross-sections from each sampling site (SS1, SS2 and SS3) using ESEM.

Figure 8. ESEM images of bioconstructive and bioweathering features on chip top surfaces and cross-sections. All are BSE images unless stated otherwise. The coloured dots represent the position where EDS spectra were obtained. A) Bioconstructions on the top surface of SS1, particularly mineralised filaments; B) Biological pitting and etching in the cross-section of SS1; C) Dissolution features (black arrows) and boring (black square) in cross-section of SS1; D) Foraminifera on the top-surface of SS2. The black arrow indicates white creamy deposits (that in the BSE image have a dark grey colour); E) Two foraminifera on the top surface of SS2; F) White creamy deposits on the top surface of SS2 (these white deposits are dark in BSE); G) Manganese oxides in the cross-section of SS3 (SE image); J) Acicular crystals of Ca-phosphate on the top surface of SS3; K) Cubic crystals of Ca-phosphate on the top surface of SS3; I) Microboring caused by endolithic organisms on mineral grains in the cross-section of SS3.

Figure 9. ESEM-BSE images of representative cross-sections from the three sampling sites (SS1, SS2 and SS3). A) salt penetration band (SPB) is observed on the surface of SS1; B) biological pitting (due to microalgal growth) is visible (black arrows); C) SS2 is characterised by several layers of calcite with different porosity and permeability. Borings are clearly visible along the cross-section in the second layer; D) the top surface of SS3 is characterised by cubic Ca-phosphates and black coating of Mn-Fe oxides, whereas the inner part is made of carbonates enriched with Mg and acicular Ca-phosphates.

Table 3. Short description of the main results for the three sampling sites from Lighthouse Cave, regarding rock characteristics and properties, weathered rind, dominant microbial features, and microtopography values.

Table 4. Statistical results obtained using the ANOVA test for the occurrence of biological features as observed by stereomicroscopy. df W = degrees of freedom within group; df B = degrees of freedom between groups; ms W = mean square variance within group; ms B = mean square variance between groups; F = ratio of variance; *P* = significance.

Table 5. Student's *t*-test (two tailed test: two-samples assuming unequal variance) analysis of bioconstructive features observed using ESEM in each sampling site.

Table 6. Student's *t*-test (two tailed test: two-samples assuming unequal variance) analysis of bioweathering features observed using ESEM in each sample.

519 **References**

520 Audra, P., De Waele, J., Bentaleb, I., Chroňáková, A., Krištůfek, V., D'Angeli, I.M., Carbone, C.,
521 Madonia, G., Vattano, M., Scopelliti, G., Cailhol, D., Vanara, N., Temovski, M., Bigot, J.-Y.,
522 Nobécourt, J.-C., Galli, E., Rull, F., Sanz-Arranz, A., 2019. Guano-related phosphate-rich
523 minerals in European caves. International Journal of Speleology 48 (1), 75-105.

524 Barton, H.A., Northup, DE., 2007. Geomicrobiology in cave environments: past, current and future
525 perspectives. Journal of Cave and Karst Studies 69 (1), 163-178.

526 Bell, R.A., 1993. Cryptoendolithic algae of hot semiarid lands and deserts. Journal of Phycology 29,
527 133-139.

528 Black, M., 1933. The algal sediments of Andros Island, Bahamas. Royal Society of London,
529 Philosophical Transaction 244, 271-276.

530 Bontognali, T.R.R., D'Angeli, I.M., Tisato, N., Vasconcelos, C., Bernasconi, S.M., Grau Gonzales,
531 E.R., De Waele, J., 2016. Mushroom speleothems: Stromatolites that formed in the absence of
532 phototrophs. Frontiers in Earth Science 4, 49.

533 Bourke, M., Viles, H., Nicoli, J., Lyew-Ayee, P., Ghent, R., Holmlund, J., 2008. Innovative
534 applications of laser scanning and rapid prototype printing to rock breakdown experiments. Earth
535 Surface Processes and Landforms 33,1614-1621.

536 Burne, R.V., Moore, L.S., 1987. Microbialites: organosedimentary deposits of benthic microbial
537 communities. Palaios 2 (3), 241-254.

538 Carew, J.L., Mylroie, J.E., 1985. The Pleistocene and Holocene stratigraphy of San Salvador Island,
539 Bahamas, with reference to marine and terrestrial lithofacies at French Bay. In: Curran, H.A.
540 (Ed.), Pleistocene and Holocene Carbonate Environments on San Salvador Island, Bahamas.
541 Geological Society of American Annual Meeting. Field Trip guide, Field Trip 2, CCFL
542 Bahamian Field Station, Fort Lauderdale, 11-61.

543 Coombes, M.A., Naylor, L.A., Thompson, R.C., Roast, S.D., Gómez-Pujol, L., Fairhurst, R.J.,
544 2011. Colonization and weathering of engineering materials by marine microorganisms: an SEM
545 study. Earth Surface Processes and Landforms 36, 582-593.
546 Coombes, M.A., La Marca, E.C., Naylor, L.A., Piccini, L., De Waele, J., Sauro, F., 2015. The
547 influence of light attenuation on the biogeomorphology of a marine karst cave: A case study of
548 Puerto Princesa Underground River, Palawan, the Philippines. Geomorphology 229,125-133.
549 Contos, A.K., James, J.M., Heywood, B., Pitt, K., Rogers, P., 2001. Morphoanalysis of bacterially
550 precipitated subaqueous calcium carbonate from Weebubbie Cave, Australia.
551 Geomicrobiological Journal 18, 331-343.
552 Cox, G., James, J.M., Osborne, R.A.L., Leggett, K.E.A., 1989a. Stromatolitic crayfish-like
553 stalagmites. Proceedings University of Bristol Speleological Society 18, 339-358.
554 Cox, G., James, J.M., Leggett, K.E.A., Osborne, R.A.L., 1989b. Cyanobacterially deposited
555 speleothems: subaerial stromatolites. Geomicrobiological Journal 7, 245-252.
556 Crump, M.A., Gamble, D.W., 2004. Climate-deriving water budget and synoptic-scale precipitation
557 pattern analysis. In: Lewis, R.R., Panuska, B. (Eds.), Proceedings of the 11th symposium on the
558 Geology of the Bahamas and other Carbonate regions 2002. Gerace Research Centre, College of
559 the Bahamas, San Salvador, 127-134.
560 D'Angeli, I.M., Sanna, L., Calzoni, C., De Waele, J., 2015a. Uplifted flank margin caves in
561 telogenetic limestones in the Gulf of Orosei (Central-East Sardinia—Italy) and their
562 palaeogeographic significance. Geomorphology 231, 202-211.
563 D'Angeli, I.M., De Waele, J., Melendres, O.C., Tisato, N., Sauro, F., Gonzales, E.R.G., Bernasconi,
564 S.M., Torriani, S., Bontognali, T.R.R., 2015b. Genesis of folia in a non-thermal epigenic cave
565 (Matanzas, Cuba). Geomorphology 228, 526-535.
566 De Waele, J., D'Angeli, I. M., Tisato, N., Tuccimei, P., Soligo, M., Ginés, J., Ginés, A., Fornós, J.J.,
567 Villa, I.M., Grau González, E.R., Bernasconi, S.M., Bontognali, T.R.R., 2017. Coastal uplift rate

568 at Matanzas (Cuba) inferred from MIS 5e phreatic overgrowths on speleothems. Terra Nova 29
569 (2), 98-105.
570 De Waele, J., D'Angeli, I. M., Bontognali, T., Tuccimei, P., Scholz, D., Jochum, K. P., Columbu,
571 A., Bernasconi, S.M., Fornós, J.J., Grau González, E.R., Tisato, N., 2018. Speleothems in a north
572 Cuban cave register sea-level changes and Pleistocene uplift rates. Earth Surface Processes and
573 Landforms 43 (11), 2313-2326.
574 Dotson, K.E., Schelble, R.T., Spilde, M.N., Crossey, L.J., Northup, D.E., 1999. Geochemistry and
575 mineralogy of corrosion residues, Lechuguilla and Spider Caves, Carlsbad Caverns National
576 Park, New Mexico, Biogeochemical processes in an extreme environment. Geological Society of
577 America Abstract Programme 31, A154.
578 Friedmann, E.I., 1982. Endolithic microorganisms in the Antartic cold desert. Science 215, 1045-
579 1053.
580 Frierdich, A.J., Catalano, J.G., 2012. Distribution and speciation of trace elements in iron and
581 manganese oxide cave deposits. Geochimica et Cosmochimica Acta 91, 240-253.
582 Giaccio, B., Galadini, F., Sposato, A., Messina, P., Moro, M., Zreda, M., Cittadini, A., Salvi, S.,
583 Todero, A., 2002. Image processing and roughness analysis for exposed bedrock fault planes as a
584 tool for paleoseismological analysis: results from the Campo Felice fault (central Apennines,
585 Italy). Geomorphology 49, 281-301.
586 Gomez-Pujol, L., Fornós, J.J., Swantesson, J.O.H., 2006. Rock surface millimeter-scale roughness
587 and weathering of supratidal Mallorcan carbonate coasts (Balearic Islands). Earth Surface
588 Processes and Landforms 31, 1792-1801.
589 Gradzínskí, M., Szulc, J., Smyk, B., 1997. Microbial agents of moonmilk calcification. In: Jeannin,
590 P.Y. (Ed.), Proceeding 12th International Congress of Speleology, La Chaux-de-Fonds
591 (Switzerland), Vol. 1, 275-278.

592 Gulley, J.D., Martin, J.B., Moore, P.J., Brown, A., Spellman, P.D., Ezell, J., 2015. Heterogeneous
593 distributions of CO_2 may be more important for dissolution of karstification in coastal eogenetic
594 limestone than mixing dissolution. Earth Surface Processes and Landforms 40, 1057-1071
595 Gulley, J.D., Martin, J.B., Brown, A., 2016. Organic carbon inputs, common ions and degassing:
596 rethinking mixing dissolution in coastal eogenetic carbonate aquifers. Earth Surface Processes
597 and Landforms 41, 2098-2110.
598 Harris, J., Mylroie, J., Carew, J., 1995. Banana holes: unique karst features of the Bahamas.
599 Carbonates and Evaporites 10, 215-224.
600 Hill, C.A., 1987. Geology of Carlsbad Cavern and other caves in the Guadalupe Mountains, New
601 Mexico. New Mexico Bureau of Mines and Mineral Resources Bulletin 117, 1-150.
602 Hill, C.A., Forti, P., 1997. Cave minerals of the world, 2nd edition Huntsville, AL, National
603 Speleological Society: 463 pp.
604 Hiscock, H., 1996. Marine Nature Conservation Review: Rationale and Methods. Joint Nature
605 Conservation Committee, Peterborough.
606 Howarth, L.M., Wood, H.L., Turner, A.P., Beukers-Stewart, B.D., 2011. Complex habitat boosts
607 scallop recruitment in a fully protected marine reserve. Marine Biology 158, 1767-1780.
608 James, N.P., Choquette, P.W., 1984. Diagenesis 9: limestones – meteoric diagenetic environment.
609 Geosciences Journal, Canada 11, 161-194.
610 Jones, M., Pinn, E., 2006. The impact of a macroalgal mat on benthic diversity in Poole Harbour.
611 Marine Pollution Bulletin 53, 63-71.
612 Kindler, P., Mylroie, J.E., Curran, H.A., Carew, J.L., Gamble, D.W., Rothfus, T.A., Savarese, M.,
613 Sealey, N.E., 2010. Geology of the Central Eleuthera, Bahamas: A field Trip guide. Gerace
614 Research Centre, San Salvador, 74 pp.
615 Kourampas, N., Shipton, C., Mills, W., Tibesasa, R., Horton, H., Horton, M., Prendergast, M.,
616 Crowther, A., Douka, C., Faulkner, P., Picornell, L., Boivin, N., 2015. Late Quaternary

speleogenesis and landscape evolution in a tropical carbonate island: Pango la Kuumbi (Kuumbi Cave), Zanzibar. International Journal of Speleology 44 (3), 293-314.

Labourdette, R., Lascu, I., Mylroie, J., Roth, M., 2007. Process-like modeling of flank margin caves: from genesis to burial evolution. Journal of Sedimentary Research 77 (11), 965-979.

Lozano, R.P., Rossi, C., 2012. Exceptional preservation of Mn-oxidizing microbes in cave stromatolites (El Soplao, Spain). Sedimentary Geology 255, 42-55.

Lundberg, J., McFarlane, D.A., 2011. A note on the occurrence of a crayback stalagmite at Niah Caves, Borneo. International Journal of Speleology 40 (1), 39-43.

Lundberg, J., McFarlane, D.A., 2012. Post-speleogenetic biogenic modification of Gomantong Caves, Sabah, Borneo. Geomorphology 157, 153-168.

Matsuoka, N., 2001. Microgelivation versus Macrogelivation: towards bridging the gap between laboratory and field frost weathering. Permafrost Periglacial Processes Journal 12, 299-313.

McGee, D.K., Wynn, J.G., Onac, B.P., Harries, P.J., Rothfus, E.A., 2010. Tracing groundwater geochemistry using $\delta^{13}C$ on San Salvador Island (southern Bahamas): implications for carbonate island hydrogeology and dissolution. Carbonates Evaporites 25, 91-105.

Mejía-Ortíz, L.M., Pipan, T., Culver, D.C., Sprouse, P., 2018. The blurred line between photic and aphotic environments: a large Mexican cave with almost no dark zone. International Journal of Speleology 47 (1), 69-80.

Meyerhoff, A.A., Hatten, C.W., 1974. Bahamas salient of North America: Tectonic framework, stratigraphy, and petroleum potential. American Association of Petroleum Geology Bulletin 58**,** 1201-1239.

Miller, A.Z., Dionísio, A., Sequeira Braga, M.A., Hernández-Mariné, M., Afonso, M.J., Maralha, V.S.F, Herrera, L.K., Raabe, J., Fernàndez-Cortès, A., Cuezva, S., Hermosin, B., Sanchez-Moral, S., Chaminé, H., Saiz-Jimenez, C., 2012. Biogenic Mn oxide minerals coating in a subsurface granite environments. Chemical Geology 322-323, 181-191.

642 Miller, A.Z., Pereira, M.F.C., Calaforra, J.M., Forti, P., Dionísio, A., Saiz-Jimenez, C., 2014.
643 Siliceous speleothems and associated microbe-mineral interactions from Ana Heva lava tube in
644 Easter Island (Chile). Geomicrobiology Journal 31, 236–245.
645 Miller, A.Z., Garcia-Sanchez, A.M., Martin-Sanchez, P.M., Costa Pereira, M.F., Spangenberg, J.E.,
646 Jurado, V., Dionísio, A., Afonso, M.J., Iglésias Chaminé, H.I., Hermosin, B., Saiz Jimenez, C.,
647 2018. Origin of abundant moonmilk deposits in a subsurface granitic environment.
648 Sedimentology 65, 1482-1503.
649 Moses, C., Robinson, D., Barlow, J., 2014. Methods for measuring rock surface weathering and
650 erosion: A critical review. Earth-Science Reviews 135, 141-161.
651 Mylroie, J.E., 2014. Field Guide to the geology and karst geomorphology of San Salvador Island
652 and the Eleuthera Island field trip, 102 pp.
653 Mylroie, J.E., Carew, J.J., 1988. Solution conduits as indicators of late Quaternary sea level
654 position. Quaternary Science Reviews 7 (1), 55-64.
655 Mylroie, J.E., Carew, J.L., 1990. The flank margin model for dissolution cave development in
656 carbonate platforms. Earth Surface Processes and Landforms 15**,** 413-424.
657 Mylroie, J.E., Carew, J.L., 1995. Karst development in carbonate islands. In: Unconformities and
658 porosity in carbonate strata. In: Budd, D.A., Saller, H.A., Harris, P.M. (Eds.), American
659 Association of Petroleum Geology Bulletin 63, 55-76.
660 Mylroie, J.R., Mylroie, J.E., 2007. Development of the Carbonate Island Karst Model. Journal of
661 Cave and Karst Studies 69 (1), 59-75.
662 Mylroie, J.E., Jenson, J.W., Taborosi, D., Jocson, J.M.U., Vann, D.T., Wexel, C., 2001. Karst
663 features of Guam in terms of a general model of carbonate island karst. Journal of Cave and
664 Karst Studies 63 (1), 9-22.
665 Mylroie, J.E., Mylroie, J.R., Nelson, C.S., 2008. Flank margin cave development in telogenetic
666 limestones of New Zealand. Acta Carsologica 37, 15-40.

667 Naylor, L.A., Viles, H.A., 2002. A new technique for evaluating short-term rates of coastal
668 bioerosion and bioprotection. Geomorphology 47 (1), 31-44.
669 Naylor, L.A., Coombes, M.A., Viles, H.A., 2012. Reconceptualising the role of organisms in the
670 erosion of rock coasts: a new model. Geomorphology 157-158, 17-30.
671 Nicholson, D.T., 2001. Pore properties as indicator of breakdown mechanism in experimentally
672 weathered limestones. Earth Surface Processes and Landforms 26, 819-838.
673 Northup, D.E., Lavoie, K.H., 2001. Geomicrobiology of Caves: a review. Geomicrobiology Journal
674 18, 199-222.
675 Northup, D.E., Dahm, C.N., Melim, L.A., Spilde, M.N., Crossey, L.J., Lavoie, K.H., Mallory, L.M.,
676 Boston, P.J., Cunningham, K.I., Barns, S.M., 2000. Evidence for geomicrobiological interactions
677 in Guadalupe caves. Journal of Cave and Karst Studies 62, 80-90.
678 Northup, D.E., Barns, S.M., Yu, L.E., Spilde, M.N., Schelble, R.T., Dano, K.E., Crossey, L.J.,
679 Connolly, C.A., Boston, P.J., Natvig, D.O., Dahm, C.N. 2003. Diverse microbial communities
680 inhabiting ferromanganese deposits in Lechuguilla and Spider Caves. Environmental
681 Microbiology 5 (11), 1071-1086.
682 Onac, B.P., Tysseland, M., Bengeanu, M., Hofenpradli, A., 1997. Deposition of black manganese
683 and iron-rich sediments in Vântului Cave, Romania. Journal of Cave and Karst Studies 59, 128-
684 131.
685 Onac, B. P., Mylroie, J. E., White, W. B., 2001, Mineralogy of cave deposits on San Salvador
686 Island, Bahamas. Carbonates and Evaporites 16 (1), 8-16.
687 Otoničar, B., Buzjak, N., Mylroie, J., Mylroie, J., 2010. Flank margin cave development in
688 carbonate talus breccia facies: an example from Cres Island, Croatia. Acta Carsologica 39, 79-
689 91.
690 Panuska, B.C., Mylroie, J.E., Carew, J.L., 1999. Paleomagnetic evidence for three Pleistocene
691 paleosols on San Salvador Island. In: Curran, H.A., Mylroie, J.E. (Eds.), Proceeding of the Ninth

692 Symposium on the Geology of the Bahamas and Other Carbonate Regions, Bahamas Field
693 Station, San Salvador Island, Bahamas, 93-100.
694 Peck, S.B., 1986. Bacterial deposition of iron and manganese oxides in North American caves.
695 National Speleological Society Bulletin 48, 26-30.
696 Phillips, J.D., 2016. Biogeomorphology and contingent ecosystem engineering in karst landscapes.
697 Progress in Physical Geography 40, 503-526.
698 Popović, S., Nikolić, N., Jovanović, J., Predojević, D., Trbojević, I., Manić, L., Subakov Simić, G.,
699 2019. Cyanobacterial and algal abundance and biomass in cave biofilms and relation to
700 environmental and biofilm parameters. International Journal of Speleology 48 (1), 49-61.
701 Provencio, P., Polyak, V.J., 2001. Iron oxide-rich filaments: possible fossil bacteria in Lechuguilla
702 Cave, New Mexico. Geomicrobiology Journal 18 (3), 297-309.
703 Riquelme, C., Hathaway, J.J.M., Dapkevicius, M.D.L.E., Miller, A.Z., Kooser, A., Northup, D.E.,
704 Jurado, V., Fernandez, O., Saiz-Jimenez, C., Cheeptham, N., 2015. Actinobacterial diversity in
705 volcanic caves and associated geomicrobiological interactions. Frontiers in Microbiology 6,
706 1342.
707 Roth, M.J., 2004. Inventory and geometrical analysis of flank margin caves of Bahamas. Master
708 thesis, Mississippi State University.
709 Roth, M.J., Mylroie, J.E., Mylroie, J.R., Ersek, V., Ersek, C.C., 2006. Flank Margin Cave inventory
710 of the Bahamas. In: Davis, R.L., Gamble, D.W. (Eds.), Proceedings of the 12th Symposium on
711 the geology of the Bahamas and other carbonate regions. Gerace Research Center, San Salvador,
712 Bahamas, 153-161.
713 Ruggieri, R., De Waele, J., 2014. Lower- to Middle Pleistocene flank margin caves at Custonaci
714 (Trapani, NW Sicily) and their relation with past sea levels. Acta Carsologica 43 (1), 11–22.
715 Sand, W., 1997. Microbial mechanisms of determination of inorganic substrate – a general
716 mechanistic review. International Journal of Biodeterioration and Biodegradation 40, 183-190.

717 Spilde, M.N., Northup, D.E., Boston, P.J., Schelble, R.T., Dano, K.E., Crossey, L.J., Dahm, C.N.,
718 2005. Geomicrobiology of cave ferromanganese deposits, a field and laboratory investigation.
719 Geomicrobiology Journal 22, 99-116.
720 Spilde, M.N., Kooser, A., Boston, P.J., Northup, D.E., 2009. Speleosol: a subterranean soil. In:
721 White, W.B. (Ed.), Proceedings of the 15th International Congress of Speleology, Kerrville,
722 USA, 338-344.
723 Supko, P.R., 1977. Subsurface dolomite, San Salvador, Bahamas. Journal of Sedimentary Petrology
724 47, 213-220.
725 Tisato, N., Torriani, S., Monteux, S., Sauro, F., De Waele, J., Tavagna, M.L., D'Angeli, I.M.,
726 Chailloux, D., Renda, M., Eglinton, T.I., Bontognali, T.R.R., 2015. Microbial mediation of
727 complex subterranean mineral structures. Scientific Reports, 5, 15525.
728 Tomczyk-Żak, K., Zielenkiewicz, U., 2016. Microbial diversity in caves, Geomicrobiology Journal
729 33 (1), 20-28.
730 Tuğrul, A., 2004. The effect of weathering on pore geometry and compressive strength of selected
731 rock types from Turkey. Engineering Geology 75, 215-227.
732 Underwood, A.J., 1997. Experiments in Ecology – Their logical design and interpretation using
733 Analysis of Variance. Cambridge University Press, Cambridge.
734 Vacher, H.L., Mylroie, J.E., 2002. Eogenetic karst from the perspective of an equivalent porous
735 medium. Carbonates and Evaporites 17 (2), 182-196.
736 Van Hengstum, P.J., Scott, D.B., Gröcke, D.R., Charette, M.A., 2011. Sea level controls
737 sedimentation and environments in coastal caves and sinkholes. Marine Geology 286, 35-50.
738 Viles, H.A., 2000. Recent Advances in field and experimental studies of rock weathering. Zeitshrift
739 für geomorphologie Supplementband 120, 343-368.
740 Viles, H.A., 2012. Microbial Geomorphology: a neglected link between life and landscape.
741 Geomorphology 157-158, 6-16.

742 Waterstrat, W.J., Mylroie, J.E., Owen, A.M., Mylroie, J.R., 2010. Coastal caves in Bahamian eolian
743 calcarenites: differentiating between sea caves and flank margin caves using quantitative
744 morphology. Journal of Caves and Karst Studies 72 (2), 61–74.
745 White, S., Webb, J.A., 2015. The influence of tectonics on flank margin cave formation on a
746 passive continental margin: Naracoorte, Southeastern Australia. Geomorphology 229, 58-72.
747 Whitehouse, D., 2012. Surface and their measurement. Kogan Page Science Paper Edition, 389 pp.
748 Williams, R.B.G., Robinson, D.A., 1998. Weathering of sandstone by alunogen and alum salts.
749 Quaternary Journal of Engineering Geology 31, 369-373.
750 Winkler, E.M., 1997. Rock and Stone. Stone in Architecture. Springer, 1-31.
751 Winkler, T.S., Van Hengstum, P.J., Horgan, M.C., Donnelly, J.P., Reibenspies, J.H., 2016. Detrital
752 cave sediments record Late Quaternary hydrologic and climatic variability in northwestern
753 Florida, USA. Sedimentary Geology 335, 51-65.
754
755